Am J Physiol Renal Physiol 297: F1391–F1398, 2009.
First published August 19, 2009; doi:10.1152/ajprenal.00261.2009.

Novel missense mutation of uromodulin in mice causes renal dysfunction with alterations in urea handling, energy, and bone metabolism

Elisabeth Kemter,[1] Birgit Rathkolb,[1] Jan Rozman,[2] Wolfgang Hans,[3] Anja Schrewe,[4] Christina Landbrecht,[1] Matthias Klaften,[3] Boris Ivandic,[4] Helmut Fuchs,[3] Valérie Gailus-Durner,[3] Martin Klingenspor,[2] Martin Hrabé de Angelis,[3] Eckhard Wolf,[1] Ruediger Wanke,[5] and Bernhard Aigner[1]

[1]*Chair for Molecular Animal Breeding and Biotechnology and Laboratory for Functional Genome Analysis, Gene Center, and* [5]*Institute of Veterinary Pathology, Center for Clinical Veterinary Medicine, Ludwig-Maximilians-Universität Munich, Munich;* [2]*Molecular Nutricial Medicine, Else-Kröner-Fresenius Center, Technische Universität München, Freising-Weihenstephan;* [3]*Institute of Experimental Genetics, Helmholtz Zentrum München, Neuherberg, and Chair for Experimental Genetics, Technische Universität München, Munich; and* [4]*Department of Medicine III, Division of Cardiology, University of Heidelberg, Heidelberg, Germany*

Submitted 10 May 2009; accepted in final form 14 August 2009

Kemter E, Rathkolb B, Rozman J, Hans W, Schrewe A, Landbrecht C, Klaften M, Ivandic B, Fuchs H, Gailus-Durner V, Klingenspor M, Hrabé de Angelis M, Wolf E, Wanke R, Aigner B. Novel missense mutation of uromodulin in mice causes renal dysfunction with alterations in urea handling, energy, and bone metabolism. *Am J Physiol Renal Physiol* 297: F1391–F1398, 2009. First published August 19, 2009; doi:10.1152/ajprenal.00261.2009.—Uromodulin-associated kidney disease is a heritable renal disease in humans caused by mutations in the uromodulin (*UMOD*) gene. The pathogenesis of the disease is mostly unknown. In this study, we describe a novel chemically induced mutant mouse line termed *Umod*^{A227T} exhibiting impaired renal function. The A227T amino acid exchange may impair uromodulin trafficking, leading to dysfunction of thick ascending limb cells of Henle's loop of the kidney. As a consequence, homozygous mutant mice display azotemia, impaired urine concentration ability, reduced fractional excretion of uric acid, and a selective defect in concentrating urea. Osteopenia in mutant mice is presumably a result of chronic hypercalciuria. In addition, body composition, lipid, and energy metabolism are indirectly affected in heterozygous and homozygous mutant *Umod*^{A227T} mice, manifesting in reduced body weight, fat mass, and metabolic rate as well as reduced blood cholesterol, triglycerides, and nonesterified fatty acids. In conclusion, *Umod*^{A227T} might act as a gain-of-toxic-function mutation. Therefore, the *Umod*^{A227T} mouse line provides novel insights into consequences of disturbed uromodulin excretion regarding renal dysfunction as well as bone, energy, and lipid metabolism.

N-ethyl-*N*-nitrosourea; kidney; renal disease; *Umod*

MUTATIONS IN THE UROMODULIN (*UMOD*) gene result in a dominant heritable disease syndrome characterized by hyperuricemia, gout, alteration of urine concentrating ability, and inconstantly progressive renal failure and histological alterations of the kidneys, such as tubulointerstitial nephritis, cysts, and interstitial fibrosis (14, 26, 29). However, clinical features are variable also within affected families, irrespective of type and site of the mutation. As a consequence, different syndromes, i.e., medullary cystic kidney disease type 2 (MCKD2; OMIM 603860), familial juvenile hyperuricemic nephropathy (FJHN; OMIM 162000), and glomerulocystic kidney disease (GCKD; OMIM 609886) were defined, which were recently summarized as uromodulin-associated kidney disease or uromodulin storage disease with a proven *UMOD* mutation involved (5, 29).

Uromodulin, originally identified over 60 years ago as Tamm-Horsfall glycoprotein, is the most abundant protein in mammalian urine (25, 32). It is synthesized exclusively and abundantly in the cells of the thick ascending limb of Henle's loop (TALH) without macula densa cells (18). Once synthesized, the uromodulin precursor is processed within the endoplasmic reticulum (ER) and Golgi complex into mature glycoprotein (30). Uromodulin contains a complex glycosyl moiety with variable structure which suggests a capacity for adhesion to a variety of ligands (30). In addition, uromodulin is often involved in cast nephropathies due to its tendency to gelation (35). Uromodulin knockout mice show difficulties in clearing bacteria from the urinary bladder (4, 23) and have a tendency to form calcium oxalate stones under experimental hyperoxaluria (22). They exhibit only minor renal effects. Steady-state electrolyte handling and histological kidney structures are not different in these animals compared with wild-type mice (3).

This study describes the genetic and phenotypic analysis of the chemically induced mutant mouse line *Umod*^{A227T}. This mouse line harbors a novel missense mutation of uromodulin and exhibits a phenotype similar to uromodulin-associated kidney disease in humans. The aim of our study was to analyze the effect of the disease on renal function and urinary excretion of solutes as well as its impact on other organ systems.

MATERIALS AND METHODS

Animals, linkage analysis, and detection of the causative mutation. Line UREHR4 exhibited an increase in plasma urea which was heritable in an autosomal recessive manner. The mouse line was established within the Munich ENU mouse mutagenesis project, which was carried out on the inbred C3HeB/FeJ (C3H) genetic background. Mouse husbandry, breeding, linkage analysis, and genome-wide mapping were described previously (2). All animal experiments were carried out under the approval of the responsible animal welfare authority.

Additional fine mapping was performed using further SNP and microsatellite markers. *Umod* (NM_009470) was selected for sequence analysis as a positional candidate gene. Genotyping of mice was performed by allele-specific PCR and confirmed by restriction fragment length polymorphism (RFLP) analysis. Primer sequences are available on request.

Clinical chemical analyses. Analyses of blood and urine parameters were carried out as described previously (2, 28). Plasma creati-

Address for reprint requests and other correspondence: E. Kemter, Chair for Molecular Animal Breeding and Biotechnology, Gene Center, LMU Munich, Feodor-Lynen Str. 25, D-81377 Munich, Germany (e-mail: kemter@lmb.uni-muenchen.de).

nine values were determined enzymatically (Biomed, Oberschleissheim, Germany), while urine creatinine concentration was determined by the Jaffé method.

Analyses of urine and kidney function. Body weight, water consumption, and urine excretion were measured using metabolic cages for single mice (Tecniplast, Hohenpeissenberg, Germany). Urine osmolality was determined by freezing point depression analysis. Daily excretion of solutes was measured, and data were normalized to 25 g body wt. Creatinine clearance was calculated according to the formula creatinine clearance = $[\text{Crea}]_{24\text{h urine}} \times$ 24-h urine volume/$[\text{Crea}]_{\text{plasma}}$. Fractional excretion of a solute x (FE_x) was calculated according to the formula: $FE_x = ([x]_{24\text{h urine}} \times$ 24-h urine volume)/$([x]_{\text{plasma}} \times$ creatinine clearance) $\times$ 100. Blood samples for measurement of plasma parameters were taken 1 wk before metabolic cage analyses of the corresponding animals.

Analyses of blood pressure and heart rate. Blood pressure and heart rate were measured in conscious mice by a noninvasive computerized tail-cuff method using the MC4000 Blood Pressure Analysis Systems (Hatteras Instruments, Cary, NC) (17). Measurements were carried out on 4 consecutive days, with 15 measurement runs performed in each session.

Metabolic measurements. Indirect calorimetry was performed using an open respiratory system (SM-MARS, Sables Systems, Las Vegas, NV). The O_2 and CO_2 content of the individual animal chambers was analyzed by O_2 and CO_2 sensors. Oxygen consumption ($\dot{V}O_2$; ml $O_2 \cdot h^{-1} \cdot animal^{-1}$) and carbon dioxide production ($\dot{V}CO_2$; ml $CO_2 \cdot h^{-1} \cdot animal^{-1}$) were calculated from gas concentrations and flow rates (16). The respiratory quotient was calculated as RQ = $\dot{V}CO_2/\dot{V}O_2$. Heat production (HP) was calculated according to HP [mW] = $\dot{V}O_2 \times (4.44 + 1.43 \times \text{RQ})$ (15). The test was performed for 21 h (from 1400 CET to 1100 CET the next day) at 23°C with a 12:12-h light-dark cycle in the room (lights on 0630 CET, lights off 1830 CET). Body mass was determined before and after the measurement. Upon termination, rectal body temperature was measured.

Skeletal analysis. Dual-energy X-ray absorptiometry (DXA) and peripheral quantitative computed tomography (pQCT) analyses were performed as described (1). For pQCT analysis, the reference line for the CT scans was set at the most distal point of the femur (knee joint space). At 3.0 mm proximal from the reference line, two slices were taken at 0.25-mm intervals, and at 6.0 mm proximal from the reference line one slice was taken to give characteristic cross sections of the femoral metaphysis and diaphysis, respectively.

Morphological analysis. For determination of body and organ weights, mice were killed by bleeding from the retroorbital sinus under ether anesthesia. Organs were dissected, blotted dry on tissue paper, and weighed to the nearest 0.1 mg.

Histological analyses of kidneys were performed as described previously (2). Staining of histological kidney sections included hematoxylin and eosin (H&E), Giemsa, and Masson-Trichrome. Immunohistochemistry was performed with a polyclonal goat antiserum against human uromucoid (1:500; MP Biomedicals, Illkrich, France). For electronmicroscopic analysis, kidneys were fixed with 3% glutaraldehyde in PBS (pH 7.2) via orthograde vascular perfusion, and 1-mm^3 samples of the renal cortex were postfixed by immersion in the same fixative for 1 day and processed as described (2).

Western blot analyses of urine samples. Twenty-four-hour urine samples, standardized for equal creatinine levels, were denatured by boiling after addition of β-mercaptoethanol and loaded on 8% SDS-polyacrylamide minigels. Blotting and immunodetection were performed as described (20). For detection of urinary uromodulin, goat antiserum against human uromucoid (1:500; MP Biomedicals) was used. Signal intensities were quantified using ImageQuant (GE Healthcare, Munich, Germany).

Statistical analysis. Data are shown as means ± SD. Data were analyzed by using an unpaired Student's *t*-test. Mass dependent energy metabolism variables were analyzed using generalized linear models including sex, genotype, and body mass as effects.

RESULTS

Establishment of Umod^{A227T} mutant mouse line. Generation of the chemically induced mutant mouse line UREHR4 and genome-wide linkage analysis to determine the chromosomal region of the causative mutation were described previously (2). The mouse line exhibited increased plasma urea levels, which was heritable in an autosomal recessive manner. The causative mutation was linked to a single chromosomal site on chromosome 7 between 125.2 (rs3690100) and 134.8 Mb (rs31285172). The probability of the existence of confounding nonsegregating mutations in this chromosomal region is $P < 0.001$ (19). Sequence analysis of *Umod* cDNA, whose gene is located at 126.6 Mb on chromosome 7, revealed a G→A transversion in exon 3 at nt 871 (NM_009470) (Fig. 1*A*). Genotypic differentiation was enabled by allele-specific PCR reactions and was confirmed by RFLP analysis (Fig. 1, *B* and *C*). Mating of heterozygous mutant mice showed the expected Mendelian pattern of inheritance of the mutation in the offspring.

The identified mutation leads to an amino acid substitution of alanine to threonine at position 227 of uromodulin. Therefore, the line was designated as the Munich *Umod*^{A227T} mutant

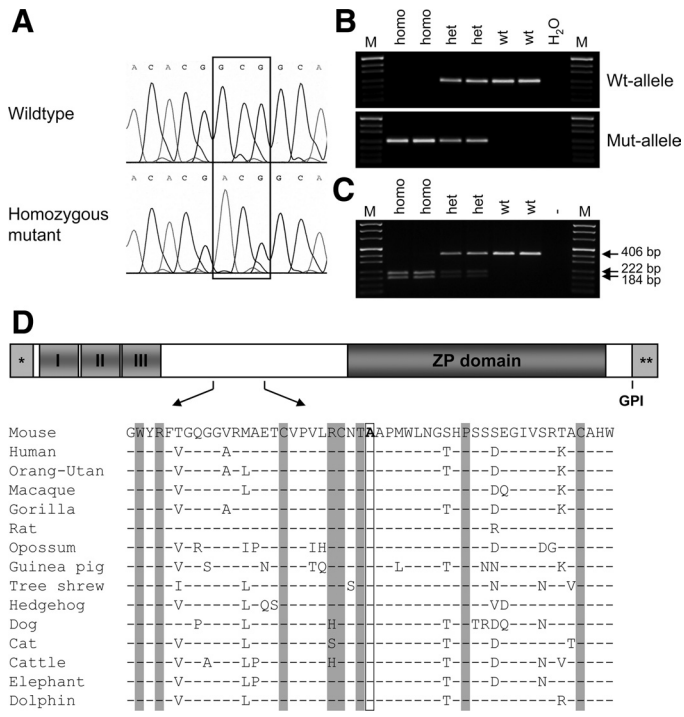

Fig. 1. Analysis of *Umod* gene sequence in wild-type and mutant mice. *A*: electropherogram of the *Umod* A227T mutation. The box shows the mutated codon, GCG (Ala) to ACG (Thr) at amino acid position 227. *B*: genotyping of mice by wild-type and mutant allele-specific PCR reaction, respectively. Homo, homozygous *Umod*^{A227T} mutant; het, heterozygous *Umod*^{A227T} mutant; wt, wild-type; M, pUC Mix 8 marker, MBI Fermentas. *C*: genotyping of mice by restriction fragment length polymorphism analysis. *Hpy*99I restriction digest of the 406 bp PCR product results in 222- and 184-bp fragments of the mutant allele. *D*: structure of uromodulin protein and sequence alignment of AA 202–252 of murine uromodulin (corresponding to AA 201–251 of the human sequence). I-III, EGF-like domains; ZP domain, zona pellucida domain; *, *N*-terminal signal peptide; **, sequence contained in propeptide and cleaved and replaced by a GPI anchor during protein processing. The alanine at position 227 is marked in bold. The positions of the different mutations reported in humans are highlighted (W202, R204, C217, R222, C223, T225, P236, C248) (6, 10, 21, 36).

mouse line. This region is relatively well conserved between species, and numerous mutations causing uromodulin-associated kidney disease in humans are located there (Fig. 1*D*).

Blood and circulation data of 4-mo-old adult Umod^{A227T} mutant mice. Plasma creatinine and urea levels were strongly increased in homozygous mutants and moderately increased in heterozygotes of both genders compared with their wild-type littermate controls (Table 1). A moderate increase in plasma calcium concentrations was detected in homozygous mutant males. Female homozygotes exhibited significantly increased uric acid levels in plasma. Cholesterol, triglycerides, and nonesterified fatty acids (NEFA) were decreased in mutants of both genders. Plasma concentration of the N-terminal fragment of pro-atrial natriuretic peptide (Nt-proANP) tended to be increased in homozygous mutants. No genotype-specific difference was seen in blood pressure and heart rate (age of mice analyzed: 12–15 wk; $n = 10$/genotype and gender; data not shown).

Blood data of 2-wk-old juvenile Umod^{A227T} mutant mice. No alterations in plasma creatinine and urea levels were detected in 2-wk-old homozygous mutant and heterozygous mutant mice of both genders compared with their age-matched wild-type littermate controls ($n = 4$–12/genotype and gender; data not shown). Plasma cholesterol and triglyceride levels tended to be decreased in female heterozygotes (Student's *t*-test vs. wild-type: $P < 0.05$ and $P < 0.01$, respectively), but not in female homozygous mutant and male mutant mice compared with their sex-matched wild-type littermate controls.

Urine excretion and concentration ability of 3- to 4-mo-old Umod^{A227T} mutant mice. A 1.5-fold increase in daily urine volume and a significant decrease in urine osmolality were detected in adult homozygous mutant mice compared with wild-type controls (Table 2). Although urine-to-plasma ratios of sodium and potassium were significantly decreased (Fig. 2*A*), fractional excretions were fairly unchanged and daily urinary excretions were only moderately increased in homozygous males (Fig. 2*B*). In contrast, urine-to-plasma ratios of urea and uric acid were decreased two- to threefold (Fig. 2*A*), and also fractional excretions were decreased twofold (Fig. 2*B*). In addition, homozygotes of both genders exhibited a threefold increased excretion of calcium (Table 2). Also, daily urinary excretion of magnesium was significantly increased in homozygous males ($P < 0.001$), and this tendency was also seen in homozygous females ($P = 0.075$ vs. wild-type). Urinary excretion of uromodulin was markedly decreased in homozygous mutant mice of both genders (Fig. 2*C*). The uromodulin signals detected in urine of homozygous mutant and heterozygous mutant mice corresponded to the size of the wild-type uromodulin band.

Despite deprivation of drinking water, homozygotes still excreted 40% more urine than wild-type controls (males: $P < 0.01$, females: $P = 0.06$), whereas urine osmolality remained significantly decreased (Table 2).

Compared with wild-type controls, urinary data of heterozygotes often showed a tendency of alterations toward the direction seen in homozygous mutants.

Morphological, metabolic, and skeletal data of Umod^{A227T} mutant mice. Adult homozygous mutants of both genders had a significantly lower body weight than wild-type mice (Tables 2 and 3). Heterozygous mutants showed an intermediate state. Most relative organ weights were not significantly different between genotypes (not shown). Analysis of body composition, performed by DXA, demonstrated that fat mass and fat content (percent body fat) were significantly decreased in mutants whereas lean content (percent lean mass) was increased (Table 3).

Analysis of energy metabolism by indirect calorimetry revealed that body temperature and metabolic rate were decreased in adult mutants (Fig. 3). Both mean and minimum

Table 1. *Plasma data of 4-mo-old mice*

	Male			Female		
	Wild-Type	Heterozygous	Homozygous	Wild-Type	Heterozygous	Homozygous
Na^+, mmol/l	152.0±3.8	152.8±2.1	153.8±3.9	147.8±4.0	147.4±2.3	147.0±2.7
K^+, mmol/l	4.34±0.28	4.56±0.18	4.60±0.42	4.10±0.19	4.44±0.16‡	4.42±0.27†
Ca^{2+}, mmol/l	2.20±0.07	2.21±0.07	2.31±0.10*	2.31±0.06	2.32±0.05	2.35±0.07
Cl^-, mmol/l	108.2±3.8	109.6±2.0	109.7±3.3	107.8±1.9	107.2±2.1	106.8±2.2
Mg^{2+}, mmol/l	0.78±0.07	0.75±0.04	0.79±0.05	0.85±0.06	0.87±0.06	0.90±0.04*
P_i, mmol/l	1.40±0.30	1.08±0.19*	1.20±0.31	1.26±0.27	1.02±0.32	1.10±0.29
Total protein, g/l	52.8±2.3	52.0±1.3	53.2±3.9	53.0±2.7	51.8±1.5	52.2±2.4
Albumin, g/l	28.0±1.3	28.0±0.9	29.0±1.4	29.0±1.4	28.6±1.0	28.8±1.7
Creatinine, μmol/l	12.5±4.4	17.7±2.4†	17.8±4.3*	13.7±4.2	18.8±3.6†	21.4±5.8†
Urea, mmol/l	9.9±0.8	11.5±0.7‡	17.8±1.4‡	10.0±1.6	12.8±1.5‡	15.8±1.5‡
Uric acid, μmol/l	66.2±10.3	76.3±44.3	67.0±7.4	92.7±9.9	98.7±23.3	113.8±19.3†
Cholesterol, mmol/l	4.03±0.38	3.48±0.26†	3.64±0.40*	3.27±0.38	2.91±0.22*	2.97±0.27
Triglycerides, mmol/l	3.36±0.86	2.22±0.53†	2.29±0.65†	3.35±0.88	2.85±0.65	2.20±0.80†
NEFA, mmol/l	3.62±0.33	2.96±0.30‡	3.11±0.51*	1.44±0.19	1.28±0.26	1.33±0.11
LDH, U/l	227.4±123.7	250.8±111.0	308.5±140.0	230.2±53.7	239.3±35.1	215.2±40.8
ALAT, U/l	20.0±2.8	20.8±10.4	28.6±12.3*	22.6±4.6	20.8±3.7	21.0±5.9
ASAT, U/l	42.2±6.1	48.8±19.2	63.2±29.8*	47.2±10.2	49.6±9.4	51.2±10.9
AP, U/l	97.4±8.5	97.6±10.0	115.8±8.6‡	118.2±16.5	126.4±10.3	134.4±18.0
α-Amylase, U/l	2,262±190	2,122±146	2,162±218	2,061±146	1,977±124	2,101±155
Glucose, mmol/l	7.91±1.57	8.01±2.47	7.41±2.00	7.26±1.62	7.69±0.96	8.03±1.26
Lactate, mmol/l	12.9±1.1	12.5±0.8	13.2±1.0	11.5±1.7	12.0±0.9	11.9±0.8
Nt-proANP, nmol/l	1.87±1.03	2.31±0.61	2.64±0.60	1.54±0.51	1.77±0.46	1.97±0.35*

Values are means ± SD; $n = 6$–10/genotype and gender. P_i, inorganic phosphorus; NEFA, nonesterified fatty acid; LDH, lactate dehydrogenase (EC 1.1.1.27); ALAT, alanine aminotransferase (EC 2.6.1.2); ASAT, aspartate aminotransferase (EC 2.6.1.1); AP, alkaline phosphatase (EC 3.1.3.1); Nt-proANP, *N*-terminal pro-atrial natriuretic peptide. Student's *t*-test vs. wild-type: *$P < 0.05$, †$P < 0.01$, ‡$P < 0.001$.

Table 2. *Body weight and urine data of adult mice under basal conditions and after deprivation of drinking water for 24 h*

	Male			Female		
	Wild-Type	Heterozygous	Homozygous	Wild-Type	Heterozygous	Homozygous
Body weight, g	29.0±2.0	27.3±1.4*	26.5±1.2‡	24.0±1.9	23.6±1.3	22.5±1.6*
Drinking water ad libitum						
Water intake, ml/day	5.4±1.5	6.4±2.9	6.0±1.1	6.9±1.4	6.1±2.4	8.1±2.5
Urine volume, ml/day	1.35±0.49	1.49±0.48	2.28±0.49‡	1.77±0.42	1.91±0.54	2.65±1.21*
Urine osmolality, mosmol/kgH_2O	2,968±736	3,077±352	2,179±325†	3,517±636	3,370±635	2,420±440‡
Na^+, μmol/day	235±69	282±83	300±70*	377±50	400±68	392±93
K^+, μmol/day	505±143	579±174	703±139†	923±112	966±175	997±306
Ca^{2+}, μmol/day	2.6±1.3	3.2±1.0	8.4±2.4‡	4.1±0.4	6.2±1.2‡	13.9±5.5‡
Cl^-, μmol/day	385±105	476±126*	480±93*	626±69	633±83	604±146
Mg^{2+}, μmol/day	27.3±9.9	34.3±12.6	43.4±9.2‡	47.7±8.9	58.4±15.7*	58.7±19.4
P_i, μmol/day	219±70	211±76	232±107	283±131	354±190	265±122
Creatinine, μmol/day	4.7±1.0	5.5±1.6	6.7±1.2‡	6.2±0.7	7.0±1.4	7.0±2.2
Urea, mmol/day	2.4±0.6	2.8±0.9	3.1±0.6†	3.5±0.5	3.7±0.7	3.6±1.2
Uric acid, nmol/day	612±246	562±175	364±69†	1475±242	1234±254*	853±299‡
Glucose, μmol/day	2.7±0.7	3.1±0.8	3.1±0.6	5.5±1.6	5.0±1.1	5.8±3.8
Total protein, mg/day	10.9±3.7	11.3±3.7	12.6±3.1	8.7±2.3	9.2±3.4	4.3±1.7‡
Deprivation of drinking water for 24 h						
Urine volume, ml	0.73±0.29	0.86±0.32	1.04±0.28†	0.64±0.29	0.72±0.30	0.87±0.30
Urine osmolality, mosmol/kgH_2O	4217±763	4076±661	3132±431‡	5251±1,504	4770±872	3401±610‡

Values are means ± SD, standardized on 25-g body wt; n = 11–14/genotype and gender. Age of mice analyzed: 13–16 wk. Student's t-test vs. wild-type: *$P < 0.05$, †$P < 0.01$, ‡$P < 0.001$.

hourly rates of energy expenditure monitored over 21 h were lowest in homozygous mutants and intermediate in heterozygotes. However, correlated to body weight, this effect was diminished and only reached the level of significance in homozygotes compared with wild-type mice [not shown; generalized linear model ($\dot{V}o_2 \sim$ genotype + sex + body mass): genotype $P < 0.01$, sex $P < 0.05$, body mass $P < 0.05$]. Metabolic fuel utilization was not different as concluded from the RQ (Fig. 3).

To elucidate the long-term effect of hypercalciuria, an analysis of the skeleton was performed. DXA analysis showed that bone mineral density and bone mineral content were significantly decreased in 4-mo-old mutant animals, indicating osteopenia (Table 3). This was more pronounced in homozygous mutants than in heterozygotes. pQCT analysis of 6-mo-old mice revealed that total and cortical bone content were significantly reduced at the distal femoral metaphysis and diaphysis in homozygous male mutants, with the same tendency in females (not shown). Additionally, total, trabecular, and cortical bone density was significantly decreased at the femoral diaphysis in male homozygous mutants (same tendency in females) compared with wild-type mice.

Pathological findings in the kidney. Kidneys of 3- to 6-mo-old homozygous mutant mice appeared unremarkable by light microscopy. Immunohistochemical analysis for uromodulin demonstrated weak diffuse homogenous cytoplasmic and distinct apical membrane staining for uromodulin in the distribution of the TALH in wild-type control mice (Fig. 4*A*). In contrast, TALH cells of homozygous mutants exhibited more intense uromodulin staining, which was located intracytoplasmically in the perinuclear compartment (Fig. 4*B*). On ultrastructural evaluation, TALH cells contained intracytoplasmic inclusions composed of perinuclear stacked lamellar structures occasionally associated with ER granules (Fig. 4, *C* and *D*). These lamellar structures might represent hyperplastic bundles of the ER. In addition, the mitochondrial basal labyrinth in the periphery of the nucleus seemed to be less compact. Glomeruli and proximal tubules appeared unremarkable.

DISCUSSION

Homozygous *Umod*^{A227T} mutant mice are viable, and they grow and reproduce normally. They show a defect in the urine concentration mechanism and the excretion of urinary solutes. The causative mutation A227T is located in a relatively well-conserved region of uromodulin where also numerous mutations in humans causing uromodulin-associated kidney disease were detected. Uromodulin is a GPI-anchored glycoprotein localized at the apical membrane of TALH cells, from where it is released into urine by proteolytic cleavage (30). Therefore, correct biosynthesis and intracellular routing through the ER and Golgi complex are essential. It has been demonstrated that uromodulin mutations cause protein misfolding, leading to defective and delayed uromodulin trafficking (26, 33). This explains the observed altered immunohistochemical staining pattern of uromodulin on TALH cells as well as the electron microscopic results suggestive of a storage disease (24, 26, 33). Similar alterations of TALH cells were also observed in homozygous *Umod*^{A227T} mutant mice. In humans, heterozygous carriers of *UMOD* mutations had a lower urinary uromodulin excretion than control subjects, and mass spectrometric analyses demonstrated that urinary uromodulin corresponded to the wild-type isoform (10). As demonstrated in homozygous mutant mice, mutant *Umod*^{A227T} protein is excreted even though in a distinctly reduced amount due to altered uromodulin trafficking. Western blot analysis detected excreted mutant *Umod*^{A227T} protein with a size corresponding to wild-type uromodulin, which excludes major alterations in the glycosylation pattern. The concise glycosylation pattern has to be analyzed in more detail in further studies as the A227T-exchange generates a potentially new O-linked glycosylation site.

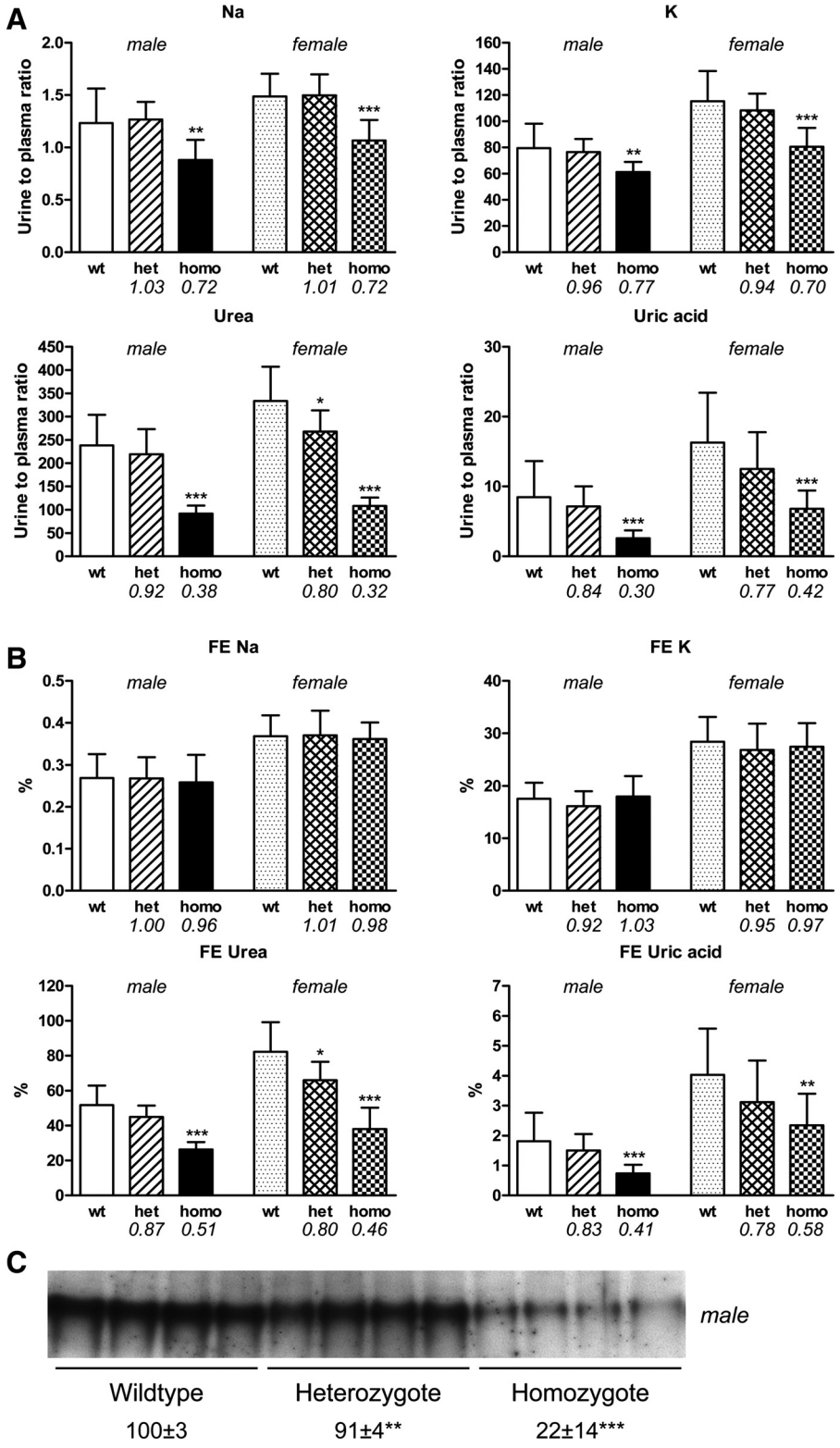

Fig. 2. Urine-to-plasma ratios, fractional excretion, and Western blot analysis of uromodulin content in urine of adult mice. *A*: urine-to-plasma ratio of sodium, potassium, urea, and uric acid was decreased in homozygous mutant mice of both genders compared with wild-type littermate controls, whereas these of urea and uric acid are more pronounced decreased. *B*: fractional excretion of sodium and potassium were fairly unchanged between genotypes. In contrast, fractional excretion of urea and uric acid were distinctly decreased in homozygous mutants of both genders compared with wild-type littermate control mice. *A* and *B*: age of mice analyzed: 13–16 wk. Values are means ± SD. Ratios relative to wild-type value are indicated in italic. n = 11–14/genotype and gender. Wt, wild-type; het, heterozygous mutant; homo, homozygous mutant. Student's t-test vs. wild-type: $^{*}P < 0.05$, $^{**}P < 0.01$, $^{***}P < 0.001$. *C*: Western blot analysis of uromodulin content in urine, normalized for creatinine, demonstrates that uromodulin excretion in urine is distinctly decreased in homozygous mutant mice compared with wild-type control mice. The uromodulin signals detected in urine of mutant mice corresponded to the wild-type uromodulin band. Signal intensities were quantified according to the mean of wild-type uromodulin signals [mean (wild-type) = 100]. Age of mice analyzed: 13–16 wk. Student's t-test vs. wild-type: $^{**}P < 0.01$, $^{***}P < 0.001$.

Homozygous *Umod*^{A227T} mutant mice exhibited alterations of renal function. So far, no direct function of uromodulin in ion transport or on urinary excretion of solutes was reported. However, a defect of uromodulin trafficking might affect the residual capacity of the ER for protein maturation in TALH cells. Furthermore, the physiological location of uromodulin on TALH cells might be required for their function. Uromodulin is colocalized with the Na^+-K^+-$2Cl^-$ cotransporter (NKCC2), a major ion transporter of TALH cells, in lipid rafts of TALH cell membranes, and NKCC2 ion transport activity is lipid raft-dependent (34). Thus the functional defects in ion transport of TALH cells might be secondary to the *Umod* mutation.

Table 3. *DXA analysis of weight- and bone-related parameters of adult mice*

	Male			Female		
	Wild-Type	Heterozygous	Homozygous	Wild-Type	Heterozygous	Homozygous
Body weight, g	32.6±2.6	29.4±1.9†	27.8±3.2†	33.2±4.1	28.8±2.5	25.2±1.6
Fat mass, units	10.8±3.4	6.2±3.0†	5.8±4.2*	21.6±5.4	11.4±7.0*	9.9±8.3*
Fat content, units × 100/g	32.8±8.3	20.8±7.8†	19.8±11.4*	65.9±16.8	39.4±24.2	37.8±31.1
Lean mass, units	14.6±2.3	16.5±1.7	15.5±3.0	16.8±2.8	15.4±2.1	16.3±1.7
Lean content, units × 100/g	45.4±8.6	56.4±7.7*	56.6±11.3*	51.7±11.7	54.2±9.0	64.9±5.7
BMD, mg/cm^2	58.2±3.2	52.2±2.7‡	51.3±5.0†	61.3±5.2	55.1±2.0*	53.2±2.6*
BMC, mg	694±141	555±135*	522±172*	666±110	590±122	474±78*
Bone content, %	2.12±0.35	1.87±0.32	1.85±0.39	2.00±0.12	2.03±0.26	1.87±0.21

Values are means ± SD; n = 9–10/genotype of males; n = 5–7/genotype of females. Age of mice analyzed: 15–18 wk. DXA, dual-energy X-ray absorptiometry; BMD, bone mineral density; BMC, bone mineral content. Student's t-test vs. wild-type: *$P < 0.05$, †$P < 0.01$, ‡$P < 0.001$.

TALH cells express numerous ion transporters, such as NKCC2, ROMK, Na^+/H^+ exchanger (NHE3), KCC4, and ClC-Kb (12). Through their coordinated interaction, these transporters are responsible for reabsorption of up to 20% of glomerular filtrate and for the ability of the kidney to dilute and concentrate urine. The urine concentration ability of homozygous mutant mice was moderately impaired, and their urine osmolality was lower. In humans, low urine osmolality was constantly found in carriers of *UMOD* mutations and some patients exhibited also mild polyuria (26). Thus TALH dysfunction caused by impaired uromodulin trafficking leads to impairment of urine concentration ability, and this cannot be totally compensated by the other segments of the nephron in mutant mice and probably also in affected humans. Furthermore, mutant uromodulin might also indirectly affect the renal reabsorption of divalent mineral cations. Thus the ion transporter NKCC2 is essential for the passive paracellular reabsorption of Ca^{2+} and Mg^{2+} (12, 13). If NKCC2-mediated ion transport is impaired, this results in hypercalciuria and hypermagnesiuria, which was observed in homozygous *Umod*^{A227T} mutant mice and might also be existent in humans with *UMOD* mutations (33). The osteopenic phenotype of homozygous *Umod*^{A227T} mutant mice is probably a long-term consequence of hypercalciuria.

Reduced fractional excretion of uric acid and the occurrence of hyperuricemia are a frequent symptom of uromodulin-associated kidney disease in humans (7, 14). We also detected reduced fractional uric acid excretion in homozygous mutant mice. Renal tubular reabsorption of urate takes place in the proximal tubule, mediated by several urate transporters (8). It was hypothesized that the intracellular uromodulin overload impairs Na^+ reabsorption by the TALH cells, leading to defective urine concentrating capacity. The resulting state of volume depletion may be compensated by increased proximal tubular reabsorption of Na^+, which is known to promote reabsorption of urate (29, 31). An absence or only moderate occurrence of hyperuricemia in *Umod*^{A227T} mutant mice may be due to preserved uricase activity in mice, which is absent in humans (8).

The combination of increased (homozygous mutant males) or fairly unchanged (homozygous mutant females) daily urea excretion and reduced fractional excretion of urea may be

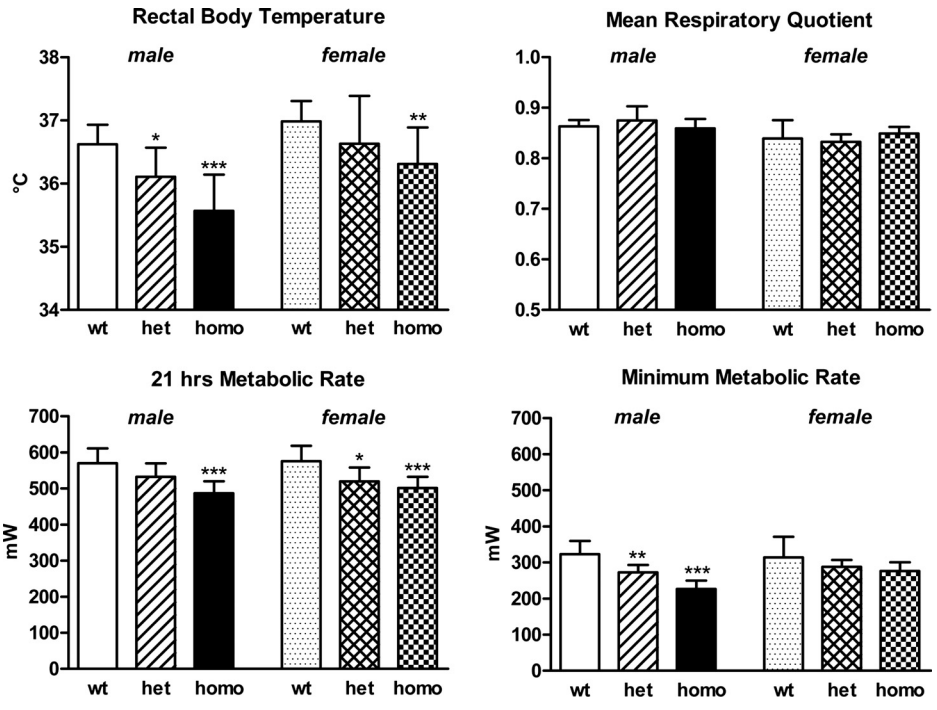

Fig. 3. Evaluation of energy metabolism by indirect calorimetry. Body temperature and metabolic rate were moderately decreased in heterozygous mutants and distinctly decreased in homozygous mutants compared with sex-matched wild-type control mice. Mean respiratory quotient was not different between genotypes, indicating that metabolic fuel utilization was not different between genotypes. Age of mice analyzed: 12–15 wk. Values are means ± SD. n = 8–10/genotype and gender. Student's t-test vs. wild-type: *$P < 0.05$, **$P < 0.01$, ***$P < 0.001$.

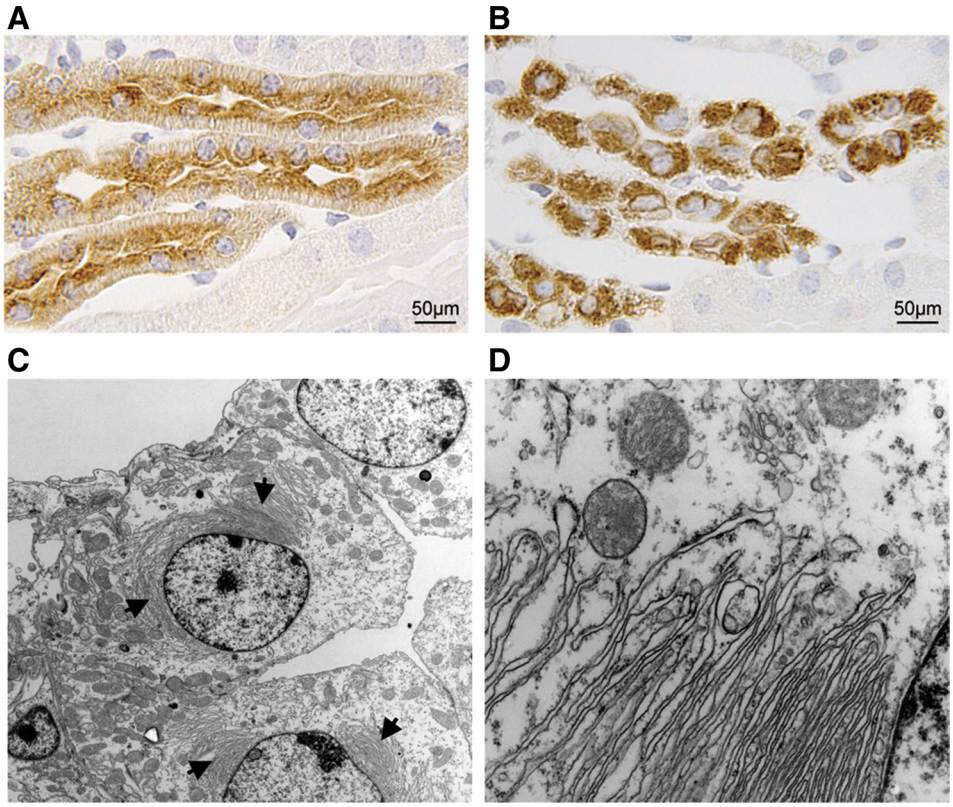

Fig. 4. Immunohistochemistry of uromodulin and transmission electron microscopy of thick ascending limb of Henle's loop (TALH) cells. *A* and *B*: representative TALH profile immunohistochemically stained for uromodulin of a 3-mo-old wild-type (*A*) and homozygous *Umod*^{A227T} mutant (*B*) mouse. In wild-type mice, weak diffuse homogeneous cytoplasmic and distinct apical membrane staining for uromodulin in TALH cells was observed. TALH cells of homozygous mutants exhibited a strong staining intensity in the cytoplasm. *C*: representative electron micrograph of TALH cells of a 6-mo-old homozygous mutant mouse; final magnification ×2,000. TALH cells contained intracytoplasmic inclusions composed of perinuclear stacked lamellar structures (arrows). Mitochondrial basal labyrinth in the surrounding of the nucleus appeared to be less compact. *D*: detail of *C* of the perinuclear cytoplasmic region of the TALH cell; final magnification ×16,000. Perinuclear stacked lamellar structures were occasionally associated with endoplasmic reticulum (ER) granules.

indicative of a urea-selective urinary concentrating defect in homozygous mutant animals. Renal urea transport is mediated by several urea transporters located at the thin descending limb or collecting duct of the nephron, or at the descending vasa recta (11, 37). As uromodulin is exclusively expressed in TALH cells, the *Umod* mutation may influence expression or activity of urea transporters indirectly as a consequence of TALH dysfunction. Urea accumulation in the inner medullary interstitium and countercurrent exchange are important features of the impact of urea in the urine concentration mechanism. If this is compromised, a urea-selective urinary concentration defect can occur (38). Also, an increase in medullary blood flow potentially causes a urea-selective concentration defect. Thus countercurrent exchange of urea between ascending and descending vasa recta might be impaired if the contact time of urea to vessel walls is too short.

Besides alterations in renal function, body composition, energy, and lipid metabolism were altered in *Umod*^{A227T} mutant mice. Thus body weight was lower in mutant mice than in wild-type controls. In addition, mutant mice accumulated less body fat. In humans, small kidney size was sometimes diagnosed by renal ultrasound analysis in carriers of *UMOD* mutations (33, 36). However, relative kidney weight was not altered in mutant mice. In addition, mutant mice exhibited a reduction in body temperature and, to a minor degree, in metabolic rate. These changes are probably secondary to the functional and structural changes in the kidney.

In humans, uromodulin-associated kidney disease is also classified as a dominant disorder. Occurrence of homozygosity for a dominant *UMOD* mutation with more pronounced clinical symptoms was reported (27). Mutations can cause loss-of-physiological function or gain-of-toxic function of the protein. In uromodulin-associated kidney disease in humans, it was hypothesized that decreased urine concentrating efficiency and impairment of water reabsorption might result from the absence of released uromodulin (33). This assumption was not confirmed by the phenotype of *Umod* knockout mice, which exhibit only minor changes in renal function (3). The phenotypic and functional alterations of *Umod*^{A227T} mutant mice suggest a gain-of-toxic function of mutant uromodulin, leading to TALH dysfunction due to disturbed uromodulin trafficking. This concept is supported by the fact that, in stably transfected immortalized TALH cells, accumulation of mutant uromodulin glycoprotein in ER induced apoptosis (9).

Taken together, the *Umod*^{A227T} mutant mouse line represents the first animal model for uromodulin-associated kidney disease with features similar to the human disease. TALH dysfunction may be caused by a defect of mutant uromodulin trafficking. We clearly demonstrated that renal consequences of the TALH dysfunction were alterations in uric acid, urea, and divalent mineral cation metabolism. In addition, consequences of an *Umod* mutation for body composition as well as for bone, energy, and lipid metabolism were for the first time systematically analyzed. Further analyses will focus on the onset and progression of this renal dysfunction and the kind of mutant uromodulin trafficking defect in the *Umod*^{A227T} mutant mouse line.

ACKNOWLEDGMENTS

We thank Angela Siebert and Lisa Pichl for excellent technical assistance on histological analyses, Elfi Holupirek, Ann-Elisabeth Schwarz, Susanne Wittich, and Miriam Backs for technical assistance on phenotypic analyses carried out at the German Mouse Clinic, and the mouse facility of the Moorversuchsgut for excellent animal care. A. Schrewe, B. Rathkolb, H.

Fuchs, J. Rozman, V. Gailus-Durner, and W. Hans are members of the German Mouse Clinic, Helmholtz Zentrum München.

GRANTS

This work was supported by the German Human Genome Project, the National Genome Research Network (01GS0850, 01GS0851, 01GS0869, and 01GS0854), and the European Commission (LSHG-2006-037188).

REFERENCES

1. **Abe K, Fuchs H, Lisse T, Hans W, Hrabe dA.** New ENU-induced semidominant mutation, Ali18, causes inflammatory arthritis, dermatitis, and osteoporosis in the mouse. *Mamm Genome* 17: 915–926, 2006.
2. **Aigner B, Rathkolb B, Herbach N, Kemter E, Schessl C, Klaften M, Klempt M, Hrabé de Angelis M, Wanke R, Wolf E.** Screening for increased plasma urea levels in a large-scale ENU mouse mutagenesis project reveals kidney disease models. *Am J Physiol Renal Physiol* 292: F1560–F1567, 2007.
3. **Bachmann S, Mutig K, Bates J, Welker P, Geist B, Gross V, Luft FC, Alenina N, Bader M, Thiele BJ, Prasadan K, Raffi HS, Kumar S.** Renal effects of Tamm-Horsfall protein (uromodulin) deficiency in mice. *Am J Physiol Renal Physiol* 288: F559–F567, 2005.
4. **Bates JM, Raffi HM, Prasadan K, Mascarenhas R, Laszik Z, Maeda N, Hultgren SJ, Kumar S.** Tamm-Horsfall protein knockout mice are more prone to urinary tract infection: rapid communication. *Kidney Int* 65: 791–797, 2004.
5. **Bleyer AJ, Hart TC, Shihabi Z, Robins V, Hoyer JR.** Mutations in the uromodulin gene decrease urinary excretion of Tamm-Horsfall protein. *Kidney Int* 66: 974–977, 2004.
6. **Bleyer AJ, Trachtman H, Sandhu J, Gorry MC, Hart TC.** Renal manifestations of a mutation in the uromodulin (Tamm Horsfall protein) gene. *Am J Kidney Dis* 42: E20–E26, 2003.
7. **Bleyer AJ, Woodard AS, Shihabi Z, Sandhu J, Zhu H, Satko SG, Weller N, Deterding E, McBride D, Gorry MC, Xu L, Ganier D, Hart TC.** Clinical characterization of a family with a mutation in the uromodulin (Tamm-Horsfall glycoprotein) gene. *Kidney Int* 64: 36–42, 2003.
8. **Choi HK, Mount DB, Reginato AM.** Pathogenesis of gout. *Ann Intern Med* 143: 499–516, 2005.
9. **Choi SW, Ryu OH, Choi SJ, Song IS, Bleyer AJ, Hart TC.** Mutant Tamm-Horsfall glycoprotein accumulation in endoplasmic reticulum induces apoptosis reversed by colchicine and sodium 4-phenylbutyrate. *J Am Soc Nephrol* 16: 3006–3014, 2005.
10. **Dahan K, Devuyst O, Smaers M, Vertommen D, Loute G, Poux JM, Viron B, Jacquot C, Gagnadoux MF, Chauveau D, Buchler M, Cochat P, Cosyns JP, Mougenot B, Rider MH, Antignac C, Verellen-Dumoulin C, Pirson Y.** A cluster of mutations in the UMOD gene causes familial juvenile hyperuricemic nephropathy with abnormal expression of uromodulin. *J Am Soc Nephrol* 14: 2883–2893, 2003.
11. **Fenton RA, Knepper MA.** Urea and renal function in the 21st century: insights from knockout mice. *J Am Soc Nephrol* 18: 679–688, 2007.
12. **Gamba G.** Molecular physiology and pathophysiology of electroneutral cation-chloride cotransporters. *Physiol Rev* 85: 423–493, 2005.
13. **Greger R.** Ion transport mechanisms in thick ascending limb of Henle's loop of mammalian nephron. *Physiol Rev* 65: 760–797, 1985.
14. **Hart TC, Gorry MC, Hart PS, Woodard AS, Shihabi Z, Sandhu J, Shirts B, Xu L, Zhu H, Barmada MM, Bleyer AJ.** Mutations of the UMOD gene are responsible for medullary cystic kidney disease 2 and familial juvenile hyperuricaemic nephropathy. *J Med Genet* 39: 882–892, 2002.
15. **Heldmaier G.** The influence of the social thermoregulation on the cold-adaptive growth of BAT in hairless and furred mice. *Pflügers Arch* 355: 261–266, 1975.
16. **Heldmaier G, Steinlechner S, Rafael J, Vsiansky P.** Photoperiodic control and effects of melatonin on nonshivering thermogenesis and brown adipose tissue. *Science* 212: 917–919, 1981.
17. **Hoelter SM, Dalke C, Kallnik M, Becker L, Horsch M, Schrewe A, Favor J, Klopstock T, Beckers J, Ivandic B, Gailus-Durner V, Fuchs H, Hrabé de Angelis M, Graw J, Wurst W.** "Sighted C3H" mice—a tool for analysing the influence of vision on mouse behaviour? *Front Biosci* 13: 5810–5823, 2008.
18. **Hoyer JR, Sisson SP, Vernier RL.** Tamm-Horsfall glycoprotein: ultrastructural immunoperoxidase localization in rat kidney. *Lab Invest* 41: 168–173, 1979.
19. **Keays DA, Clark TG, Campbell TG, Broxholme J, Valdar W.** Estimating the number of coding mutations in genotypic and phenotypic driven *N*-ethyl-N-nitrosourea (ENU) screens: revisited. *Mamm Genome* 18: 123–124, 2007.
20. **Klose R, Kemter E, Bedke T, Bittmann I, Kessler B, Endres R, Pfeffer K, Schwinzer R, Wolf E.** Expression of biologically active human TRAIL in transgenic pigs. *Transplantation* 80: 222–230, 2005.
21. **Kudo E, Kamatani N, Tezuka O, Taniguchi A, Yamanaka H, Yabe S, Osabe D, Shinohara S, Nomura K, Segawa M, Miyamoto T, Moritani M, Kunika K, Itakura M.** Familial juvenile hyperuricemic nephropathy: detection of mutations in the uromodulin gene in five Japanese families. *Kidney Int* 65: 1589–1597, 2004.
22. **Mo L, Huang HY, Zhu XH, Shapiro E, Hasty DL, Wu XR.** Tamm-Horsfall protein is a critical renal defense factor protecting against calcium oxalate crystal formation. *Kidney Int* 66: 1159–1166, 2004.
23. **Mo L, Zhu XH, Huang HY, Shapiro E, Hasty DL, Wu XR.** Ablation of the Tamm-Horsfall protein gene increases susceptibility of mice to bladder colonization by type 1-fimbriated Escherichia coli. *Am J Physiol Renal Physiol* 286: F795–F802, 2004.
24. **Nasr SH, Lucia JP, Galgano SJ, Markowitz GS, D'Agati VD.** Uromodulin storage disease. *Kidney Int* 73: 971–976, 2008.
25. **Pennica D, Kohr WJ, Kuang WJ, Glaister D, Aggarwal BB, Chen EY, Goeddel DV.** Identification of human uromodulin as the Tamm-Horsfall urinary glycoprotein. *Science* 236: 83–88, 1987.
26. **Rampoldi L, Caridi G, Santon D, Boaretto F, Bernascone I, Lamorte G, Tardanico R, Dagnino M, Colussi G, Scolari F, Ghiggeri GM, Amoroso A, Casari G.** Allelism of MCKD, FJHN and GCKD caused by impairment of uromodulin export dynamics. *Hum Mol Genet* 12: 3369–3384, 2003.
27. **Rezende-Lima W, Parreira KS, Garcia-Gonzalez M, Riveira E, Banet JF, Lens XM.** Homozygosity for uromodulin disorders: FJHN and MCKD-type 2. *Kidney Int* 66: 558–563, 2004.
28. **Schoensiegel F, Bekeredjian R, Schrewe A, Weichenhan D, Frey N, Katus HA, Ivandic BT.** Atrial natriuretic peptide and osteopontin are useful markers of cardiac disorders in mice. *Comp Med* 57: 546–553, 2007.
29. **Scolari F, Caridi G, Rampoldi L, Tardanico R, Izzi C, Pirulli D, Amoroso A, Casari G, Ghiggeri GM.** Uromodulin storage diseases: clinical aspects and mechanisms. *Am J Kidney Dis* 44: 987–999, 2004.
30. **Serafini-Cessi F, Malagolini N, Cavallone D.** Tamm-Horsfall glycoprotein: biology and clinical relevance. *Am J Kidney Dis* 42: 658–676, 2003.
31. **Sica D, Schollwerth A.** Renal handling of organic anions and cations and renal excretion of uric acid. In: *The Kidney*, edited by Brenner BM. Philadelphia, PA: Saunders, 1996, p. 607–700.
32. **Tamm I, Horsfall FL Jr.** Characterization and separation of an inhibitor of viral hemagglutination present in urine. *Proc Soc Exp Biol Med* 74: 106–108, 1950.
33. **Vylet'al P, Kublova M, Kalbacova M, Hodanova K, Baresova V, Stiburkova B, Sikora J, Hulkova H, Zivny J, Majewski J, Simmonds A, Fryns JP, Venkat-Raman G, Elleder M, Kmoch S.** Alterations of uromodulin biology: a common denominator of the genetically heterogeneous FJHN/MCKD syndrome. *Kidney Int* 70: 1155–1169, 2006.
34. **Welker P, Bohlick A, Mutig K, Salanova M, Kahl T, Schluter H, Blottner D, Ponce-Coria J, Gamba G, Bachmann S.** Renal Na^+-K^+-Cl^- cotransporter activity and vasopressin-induced trafficking are lipid raft-dependent. *Am J Physiol Renal Physiol* 295: F789–F802, 2008.
35. **Wenk RE, Bhagavan BS, Rudert J.** Tamm-Horsfall uromucoprotein and the pathogenesis of casts, reflux nephropathy, and nephritides. *Pathobiol Annu* 11: 229–257, 1981.
36. **Wolf MT, Mucha BE, Attanasio M, Zalewski I, Karle SM, Neumann HP, Rahman N, Bader B, Baldamus CA, Otto E, Witzgall R, Fuchshuber A, Hildebrandt F.** Mutations of the Uromodulin gene in MCKD type 2 patients cluster in exon 4, which encodes three EGF-like domains. *Kidney Int* 64: 1580–1587, 2003.
37. **Yang B, Bankir L.** Urea and urine concentrating ability: new insights from studies in mice. *Am J Physiol Renal Physiol* 288: F881–F896, 2005.
38. **Yang B, Bankir L, Gillespie A, Epstein CJ, Verkman AS.** Urea-selective concentrating defect in transgenic mice lacking urea transporter UT-B. *J Biol Chem* 277: 10633–10637, 2002.